Low temperature synthesis of -Al2O3 films by high-power plasma-assisted chemical vapour deposition

Kaiyun Jiang, Kostas Sarakinos, Stephanos Konstantinidis, Jochen M Schneider

Low temperature synthesis of α-Al_2O_3 films by high power plasma assisted chemical vapor deposition

Kaiyun Jiang[1], Kostas Sarakinos[1,2], Stephanos Konstantinidis[1, 3] and Jochen M. Schneider[1]

[1] Materials Chemistry (MCh), RWTH Aachen University, D-52074 Aachen, Germany

E-mail: jiang@mch.rwth-aachen.de

Abstract

In this study, we deposit Al_2O_3 films using plasma assisted chemical vapor deposition (PACVD) in an Ar-H_2-O_2-$AlCl_3$ atmosphere. A novel generator delivering approx. 4 times larger power densities than those conventionally employed in PACVD enabling efficient $AlCl_3$ dissociation in the gas phase, as well as a more intense energetic bombardment of the growing film is utilized. We demonstrate that these deposition conditions allow for the growth of dense α-Al_2O_3 films with negligible Cl incorporation and elastic properties similar to those of the bulk α-Al_2O_3 at a temperature of 560 ±10 °C.

PACS: 68.55.Nq, 68.60.Bs, 34.80.Dp
Keywords: α-Al_2O_3, PACVD, phase formation

1. Introduction

Among the various Al_2O_3 (alumina) polymorphs, the thermodynamically stable α-Al_2O_3 phase exhibits exceptional physical properties such as high hardness [1], transparency over a wide range of wavelengths [2, 3], chemical inertness and thermal stability [1, 3, 4]. Due to these properties, α-Al_2O_3 films are widely employed in surface protection and microelectronics applications. In the industrial practice, α-Al_2O_3 is grown by thermal chemical vapor deposition (CVD). A common feature of CVD grown α-Al_2O_3 is that substrate temperatures in the excess of 1000 °C are necessary to provide the film forming species with the energy required for α-Al_2O_3 phase formation [5]. These high deposition temperatures may cause the build up of thermal stresses as well as interface reactions [5] and may thus lead to poor adhesion, and thermally induced crack formation and growth [6]. Furthermore, the metallurgical properties of the substrate material may be altered by substrate heating, severely limiting the choice of substrate materials. An alternative way to provide energy to the growing film and decreasing the temperature limit for the deposition of α-Al_2O_3 is by bombardment of energetic species which are available in plasma based physical and chemical vapor deposition techniques. For instance, Wallin *et al.* [7] demonstrated the deposition of α-Al_2O_3 on hard metal substrates at a temperature as low as 650 °C using high power pulsed magnetron sputtering, while Takamura *et al.* [8] obtained this phase at a temperature of ~ 500 °C employing filtered cathodic arc. Jin *et al.* [9] reduced the temperature limit further for the growth of α-Al_2O_3 down to 280 °C by depositing Al_2O_3 films on Cr_2O_3 seed layer by rf magnetron sputtering. Kyrylov *et al.* [10] demonstrated the growth of α-Al_2O_3 at 560 °C by plasma assisted chemical vapor deposition (PACVD).

In all the above cases, and despite the substantial decrease of the temperature limit for the α-Al_2O_3 formation, the deposited films have been found to exhibit porosity [11, 12] and hence inferior elastic properties [12] compared to bulk and CVD α-Al_2O_3 [13]. In the case of films deposited by bipolar pulsed PACVD, Snyders *et al.* [11] suggested that the porosity is caused by chlorine (Cl)

[2] Present address: Plasma & Coatings Physics Division, IFM Material Physics, Linköping University, SE-581 83, Linköping, Sweden

[3] Present address: Laboratoire de Chimie Inorganique et Analytique, Université de Mons, Av. Copernic 1, 7000 Mons, Belgium

incorporation into the films, due to the insufficient disassociation of the $AlCl_3$ precursor employed during PACVD. It is known that an increase of the plasma density can also intensify the interaction of the plasma with the gas molecules and the growing film. The plasma density in turn depends on the power applied to the discharge. The PACVD discharges available so far have been operating at voltages of up to 0.9 kV [11, 12, 14], resulting in discharge power densities in the range 2 to 5 W/cm^2. In the current study we have utilized a pulsed plasma generator which is able to deliver voltages up to 1.4 kV allowing for approx. 4 times larger power densities than those achieved in the conventional PACVD processes. Using plasma characterization tools and plasma modeling we show that increasing the discharge power density values from 5 W/cm^2 to 19 W/cm^2 results in an increase of the energy and the flux of the bombarding species towards the growing film, as well as in a more efficient $AlCl_3$ dissociation. These conditions allow for the growth of dense and phase pure α-Al_2O_3 films with negligible Cl incorporation and elastic properties close to the bulk values at a temperature of 560 ± 10 °C.

2. Experimental

Films were deposited in a semi-industrial parallel plate PACVD chamber from PLATEG GmbH. The plasma was generated by applying unipolar voltage pulses (up to 1.4 kV in amplitude) with a nominal width in the range of 80 to 100 µs and a frequency of 5 kHz on two 16 cm in diameter steel electrodes. The substrates (Si (100) wafers) were placed on the cathode, while the other electrode (anode) was grounded. The power was supplied by a pulse generator developed by Ganciu *et al.* at Materia Nova R&D centre [15, 16]. The experiments were performed in an $AlCl_3$-Ar-H_2-O_2 atmosphere at a pressure of 175 Pa. The composition of the gas atmosphere was 1.2% $AlCl_3$, 14.8% Ar, 82.6% H_2 and 1.4% O_2. The substrate temperature was kept at 560 °C using an external wall heating unit. The time dependent voltage and current signals were measured using an ELDITEST GE 8115 voltage and Tektronik A6303 current probe, respectively and recorded with a Tektronik TDS 3014B digital oscilloscope. To investigate the effect of the deposition conditions on the plasma composition, *in-situ* optical emission spectroscopy (OES) was employed. The OES measurements were performed using a PLASUS apparatus equipped with a charged couple device (CCD) camera for fast spectrum acquisition. The optical fiber was assembled together with a collimating lens to an observation window located at the chamber wall 10 mm above the cathode. The emission lines intensities corresponding to Ar (750.4 nm), H (434.0 nm), Al (396.1 and 394.4 nm), and AlCl (261.4 nm) neutral species and Ar^+ ions (476.4 nm) were sampled through a quartz window. The phase composition of the Al_2O_3 films was determined by means of grazing incidence X-ray diffractometry (GIXRD) in a SIEMENS D5000 apparatus using a step size of 0.01° and an angle of incidence of 1°. Energy dispersive X-ray spectroscopy (EDX) measurements were carried out to determine the chemical composition of the deposited films. Scanning electron microscopy (SEM) was employed to study the influence of the deposition parameters on the film morphology, topography and thickness. Both EDX and SEM measurements were performed in a JEOL JSM-6480 apparatus, while for the EDX measurements an EDAX Genesis2000 detector was used. The elastic modulus and hardness of the as deposited films were measured by nanoindentation. The measurements were carried out using a Berkovich tip in a Hysitron nanoindentation system. The maximum load was 2500 µN to keep the contact depth ≤ 80 nm. The film thickness was ≥ ~ 1.0 µm. The recorded data was analyzed using the method of Oliver and Pharr [17].

3. Results and discussion

Measurements of the time dependent current (I) and voltage (U) of a discharge operating at a pulse width of 80 µs and a frequency of 5 kHz are shown in figure 1. Both current and voltage exhibit constant values during the nominal pulse on-time (80 µs). As the pulse is switched off, current and voltage decay over approx. 70 µs towards zero. In the following text the magnitudes of current and voltage refer to the values measured during the pulse on-time. The I-U curve of a discharge operating at a pulse width of 80 µs and a frequency of 5 kHz is presented in the insert in figure 2. The increase of the voltage results in a close to linear increase of the current in the voltage range from 0.5 to 1.4 kV. The vertical dotted line (insert in figure 2) separates previously studied current-voltage-range [10, 11, 18] from the range investigated here. The extension of the voltage range from 0.9 kV up to 1.4 kV results in power densities (calculated by dividing the power to the area of the

cathode) up to 19 W/cm^2, which are approx. 4 times larger than those reported previously [10, 11, 18].

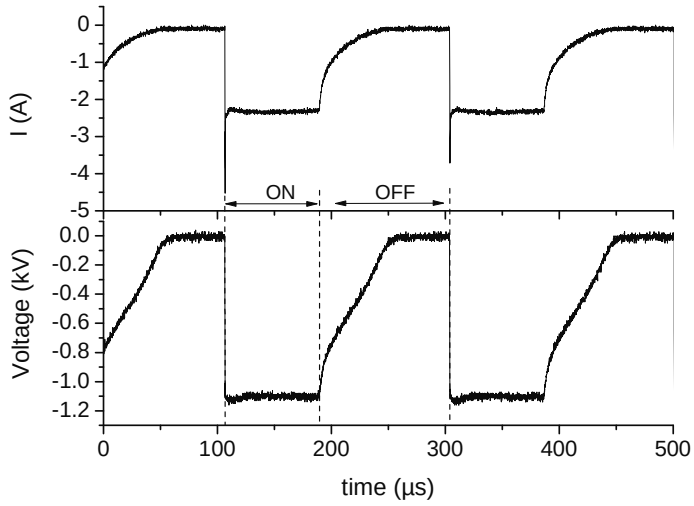

Figure 1. Time dependent cathode voltage (bottom panel) and current (top panel) of a discharge operating at a pulse width of 80 μs and a frequency of 5 kHz.

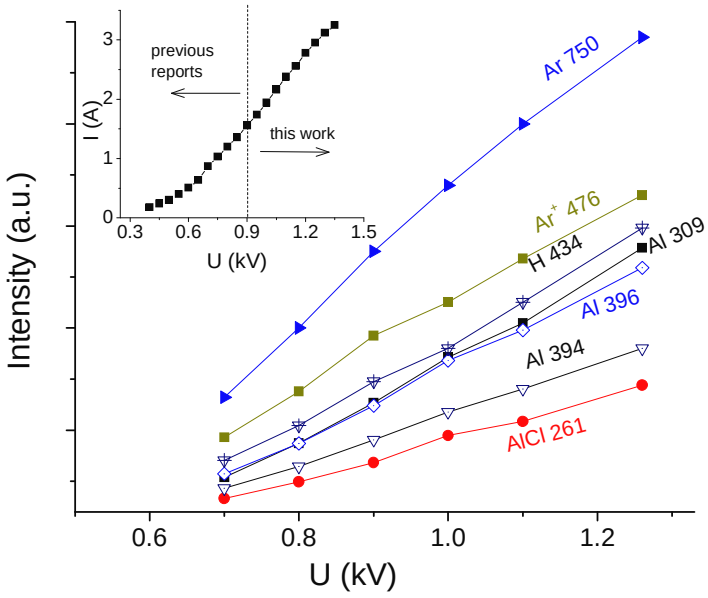

Figure 2. The intensity of the various emission lines versus the discharge voltage. The insert shows current-voltage curves recorded from the discharge operating the pulse width of 80 μs and frequency of 5 kHz.

The increase of the power density affects the plasma composition, as determined from the OES data shown in figure 2. The emission intensity of all lines increases as the discharge voltage and hence the cathode power density is increased. This may be consistent with an increase of the electron density and/or temperature, since the line intensity is proportional to the number density of excited atoms which in turn is related to the number density of the considered atoms in their ground states and to the density of the energetic particle responsible for the excitation. For instance, the energetic particle can be either an electron or an argon metastable atom (Ar*). As the voltage is increased, it is reasonable to assume that electrons will acquire more energy from the applied electric field resulting in more efficient dissociation and ionization of the plasma species. As reported in figure 2, the line intensity of the Ar 750 nm line versus the applied voltage increases. The low energy level of this

transition is related to the $3P_0$ and $3P_2$ metastable levels of the argon atom. Hence it is reasonable to assume that the increase of the line intensity indicates an increased population of metastable Ar (Ar*) as the discharge voltage is increased. Consequently, more Ar* would be available for dissociating the precursor. Zheng *et al*. reported that in an inductively coupled discharge, the presence of Ar* leads to efficient $AlCl_3$ precursor dissociation [19]. Generally, these dissociation processes can be described by the following reaction [19],

$$AlCl_3 + Ar^{*}\text{or } e^{-} \rightarrow AlCl + 2Cl + Ar \text{ or } e^{-} \quad (1)$$

which leads to the formation of Al through the reaction

$$AlCl + H \rightarrow Al + HCl \quad (2)$$

Therefore, the increase of the emission intensity of precursor related Al and AlCl lines in figure 2 should not only be attributed to the electron temperature and density increase, but also to the enhancement of the dissociation by impact of Ar*. Enhanced dissociation of BCl_3 has also been reported upon increasing the discharge power in a PACVD plasma [20].

Apart from its effect on the plasma composition, the increase of the cathode voltage to 1.3 kV leads to an up to two times larger discharge current as compared to the 0.9 kV discharge, as shown in the insert in figure 2, increasing the ion flux impinging on the growing film surface. In addition, the increase of the voltage implies a larger potential drop across the cathode sheath which in turn has implications for the energy of the ions impinging on the film. Due to the relatively high pressure of the discharge (175 Pa), ion-neutral and ion-electron collisions occur in the sheath [21]. Hence, the average ion energy is lower than the energy that can be gained by acceleration across the cathode fall. The ion energy distribution function (IEDF) was estimated based on the Davis and Vanderslice model [21] considering charge exchange collisions in the sheath. The ion energy distribution function is then given by the following expression,

$$2\lambda/L \cdot \frac{U_c \cdot dN}{N_o \cdot dU} = \frac{1}{2\sqrt{1 - U/U_c}} \cdot \exp\left[-L/\lambda \cdot (1 - \sqrt{1 - U/U_c})\right] \quad (3)$$

where L/λ is ratio between sheath thickness and mean free path for charge exchange collisions, N_0 is the total number of ions at the sheath edge and U_c is the potential difference across the sheath, i.e. the cathode potential. Here we evaluated for simplicity an Ar-H_2 plasma with a pressure of 175 Pa, since Ar and H_2 constitutes ~97% of the gas atmosphere IEDFs were calculated using Eq. (3) for pure Ar and H_2 plasmas and plotted in Fig. 3 (solid lines). For the calculation of λ in Eq. (3), the cross sections for Ar-Ar^+ (3×10^{-15} cm^2) and H_2-H_2^+ (8×10^{-16} cm^2) charge-exchange collisions were employed for Ar and H_2 plasma, respectively [22, 23]. The sheath thickness L was estimated based on the Child-Langmuir law to be 1 mm and 8 mm for Ar plasma and H_2 plasma, respectively [24]. The dashed curve in figure 3 corresponds to a plasma that consists 85% of H_2 and 15% of Ar and obtained by averaging the data from the H_2 and Ar plasma IEDFs using the respective weighting coefficients 0.85 and 0.15. These conditions are close to our experimental plasma conditions and show that the IEDF exhibits a low populated high energy tail starting from energies that correspond to a value $1/3U_c$, while the majority of the species exhibit energies that correspond to values below $1/4U_c$. Furthermore, the average ion energy determined by integration of the IEDF gives a value=0.16 U_c. Therefore, as U_c is increased from 0.9 to 1.3 kV the mean average ion energy increases from ~140 to ~200 eV. The increase of the energy and the flux of the ions towards the growing film surface result in a more intense energetic bombardment.

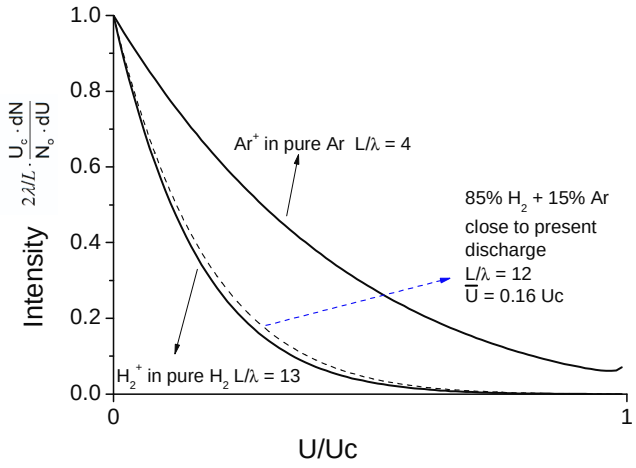

Figure 3. Ion energy distribution functions for pure Ar and H_2 plasmas (solid lines) and a plasma consisting of 85% H_2 and 15% Ar (dashed line).

In figure 4, the XRD patterns of films grown at various cathode potentials are presented. At 0.9 kV cathode potential the formation of a mixture of γ-and α-Al_2O_3 is observed. As the voltage is increased to 1.1 kV, phase pure α-Al_2O_3 films are obtained. The increase of the voltage enhances the crystallinity of the α-Al_2O_3 phase as manifested by the decrease of the full width at half maximum (FWHM) of the XRD peaks. As shown in figure 5, FWHMs of peaks at 2θ angular positions of 25.6°, 37.8° 43.3° and 52.5°, obtained by Gaussian fitting, show a decrease by 30-50%, when discharge voltage increases from 0.9 to 1.3 kV. Meanwhile, a clear appearance/separation of peaks at 2θ positions of 35.1° and 68.2° is also observed in figure 4 at a voltage of 1.1 and 1.3 kV, also indicating improved crystal quality. Furthermore, an increase of the pulse width from 80 to 100 μs (demonstrated for voltages of 1.1 and 1.3 kV in figure 4) leads to a decrease of the FHWM of the α-Al_2O_3 peaks by 5~10% (see figure 5) and subsequently to an improved crystallinity. The α-Al_2O_3 formation and improvement of crystallinity thereof can be attributed to the increased average ion energy as discussed in the pervious paragraph as well as to the increase in duration of ion bombardment enabling surface diffusion [10, 13, 18, 25]. It has to be mentioned here that due to the high plasma density at the voltage and pulse width of 1.3 kV and 100 μs, respectively, the substrate temperature was 590 ± 10 °C although no external heating was applied. The deposition temperature for all other films was 560 ± 10 °C.

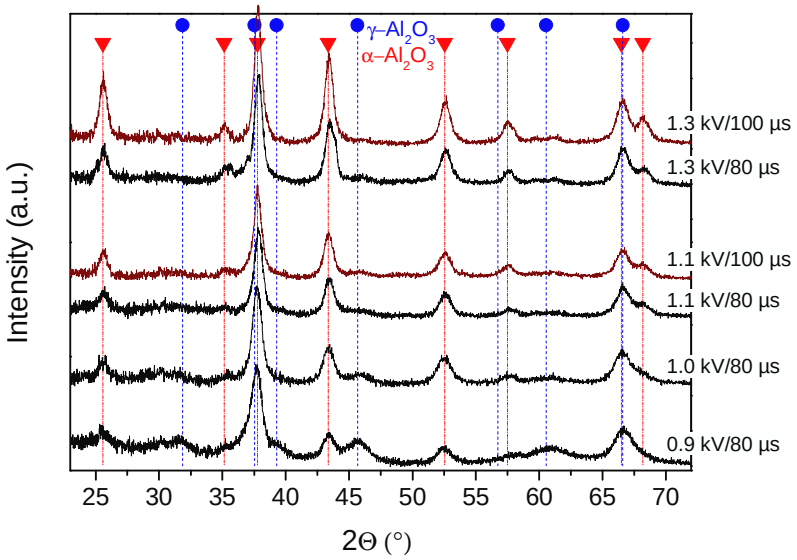

Figure 4. X-ray diffraction patterns of Al_2O_3 films deposited at various discharge voltages and pulse widths. The inverse triangles and the circles indicate the positions of the diffraction peaks associated with the presence of α- and γ-Al_2O_3, respectively.

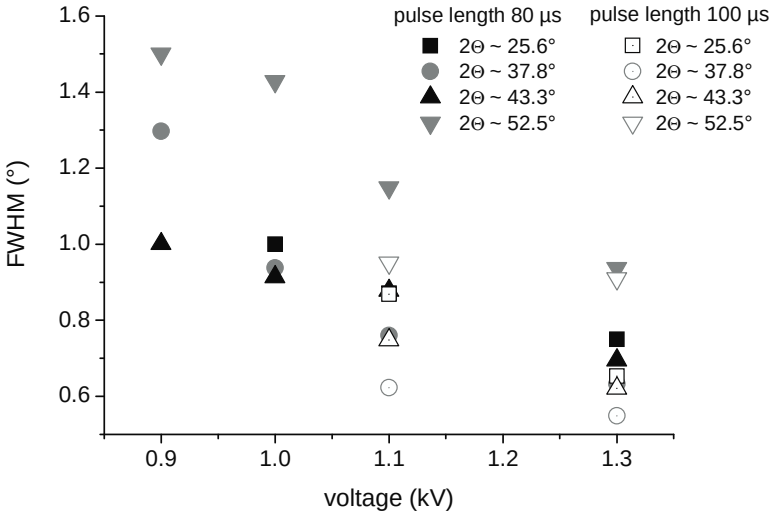

Figure 5. FWHM of chosen diffraction peaks as a function of various discharge voltages and pulse widths. Due to difficulty of peak fitting, data from sample deposited at 0.9 kV/80µs at 2θ ~25.6° is not shown.

Along with the change of the phase composition and the improvement of the crystallinity, a continuous decrease of the Cl incorporation from 1.1 to 0.5 at.% is observed as the voltage is increased from 0.9 to 1.3 kV. This may be understood by considering recently published Cl desorption data by Snyders *et al.* [11] where Cl release from α-alumina films was measured during annealing at temperatures larger than the deposition temperature. This indicates that desorption of Cl may also be expected during deposition as the energy at the surface of the growing film is increased for example due to enhanced ion bombardment. Cl desorption during growth in turn results in a decreased Cl concentration in the film, which is again consistent with the experimental observation. Recently published *ab-initio* data [11] clearly indicated that the presence of Cl destabilizes α alumina, which underlines the novelty of the here reported process where the Cl concentration could be decreased by an increase of the energy and the flux of the bombarding species towards the growing film, as well as in a more efficient $AlCl_3$ dissociation. As the discharge voltage is increased, the Cl incorporation is reduced and the formation of the α-Al_2O_3 phase is observed. Similar behavior is also obtained for the films grown at a pulse width of 100 µs. At the same time the deposition rate was found to decrease from 0.5 µm/h at a voltage of 0.9 kV to 0.36 µm/h at a voltage of 1.3 kV (pulse width of 80 µs in both cases) which could be associated with the increase of resputtering and density of deposited film at elevated voltage. On the other hand, the change of the pulse width from 80 to 100 µs had no measurable implications for the deposition rate. The elastic modulus (E) and hardness (H) of the deposited films are plotted versus the voltage in figure 6. The quantities E and H increase as the voltage is increased. The highest values for E (~380 GPa) are obtained for the films synthesized at a voltage of 1.3 kV and are very similar to that of CVD grown α-Al_2O_3 [26] and bulk ceramic α-Al_2O_3 [27] as indicated by the horizontal dashed lines in figure 6. A top view (a) and a cross sectional (b) SEM micrographs of this film are presented in the figure 7a and b, respectively. These images show a smooth surface and a dense morphology, which can be understood by the formation of phase pure α-Al_2O_3 with a density close to the bulk value, which is a consequence of ion bombardment at elevated cathode voltage, which is characterized by both a larger flux and larger average ion energy as compared to conventional PACVD synthesis approaches.

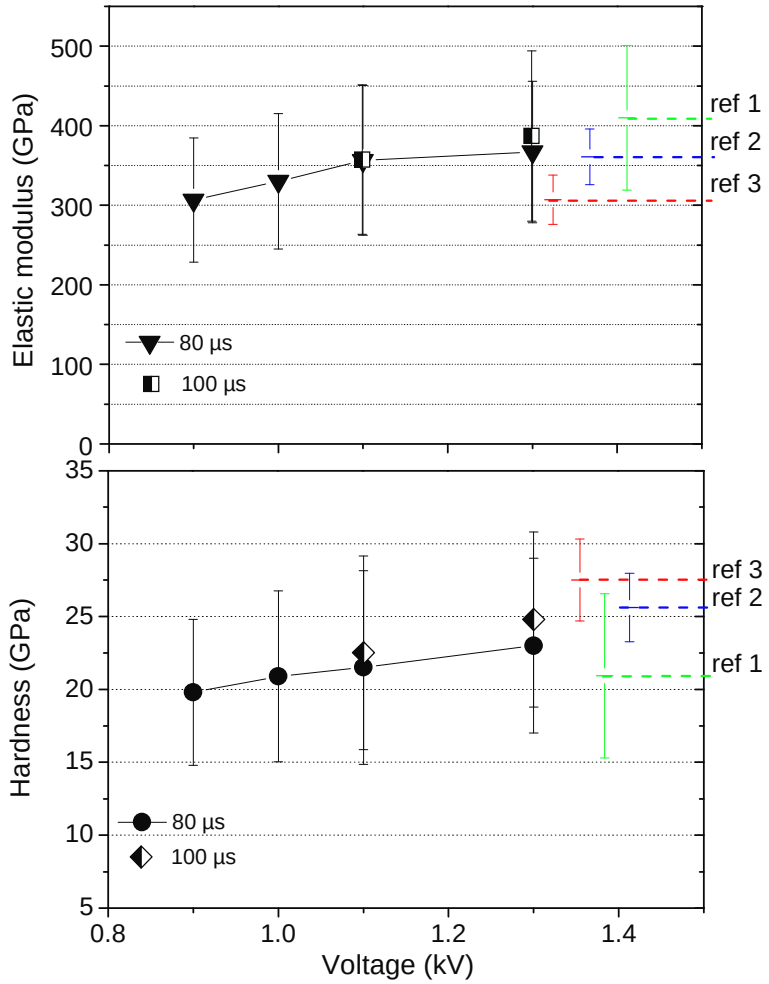

[1] Bulk nanocrystalline α-Al_2O_3[27]
[2] CVD α-Al_2O_3 film[26]
[3] RF sputtering α-Al_2O_3 film[28]

Figure 6. Elastic modulus (upper) and hardness (lower) of Al_2O_3 films as a function of the discharge voltage. The insert is a top view and the cross section SEM micrograph from a film deposited at a discharge voltage of 1.3 kV and a pulse width of 100 µs.

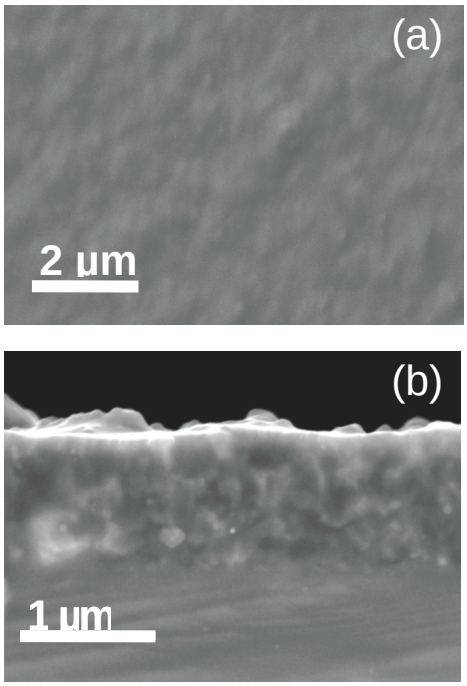

Figure 7. A top view (a) and a cross section (b) SEM micrograph from a film deposited at a discharge voltage of 1.3 kV and a pulse width of 100 µs.

5. Conclusions

In conclusion, we have employed a novel generator that allows for the operation of a PACVD discharge at approx. 4 times larger power density than those utilized conventionally. Plasma analysis and modeling indicate that the larger discharge power density enables a significant increase of $AlCl_3$ precursor dissociation efficiency, as well as an increased ion flux towards the growing film. These conditions enable the deposition of smooth and dense α-Al_2O_3 films with negligible Cl incorporation and elastic properties similar to those of the bulk α-Al_2O_3 at a growth temperature of 560 ± 10 °C.

Acknowledgments

The authors acknowledge the funding from the Deutsche Forschungsgemeinschaft (DFG) within Collaborative Research Centre (TFB) 289. S. Konstantinidis is postdoctoral researcher at the National Fund for Scientific Research (FNRS, Belgium), and he thanks The Interuniversity Attraction Poles Program of the Belgian Science Policy (Project "PSI: Fundamentals of Plasma Surface Interactions") for the financial support.

References

[1] Gitzen W H 1970 *Alumina as a Ceramic Material* (Columbus: The American Ceramic Society)

[2] Aguilar-Frutis M, Garcia M and Falcony C 1998 *Appl. Phys. Lett.* **72** 1700

[3] Holm B, Ahuja R, Yourdshahyan Y, Johansson B and Lundqvist B I 1999 *Phys. Rev. B* **59** 12777

[4] Kramer B M and Judd P K 1985 *J. Vac. Sci. Technol. A* **3** 2439

[5] Müller J, Schierling M, Zimmermann E and Neuschutz D 1999 *Surf. Coat. Technol.* **121** 16

[6] Gobel T, Menzel S, Hecker M, Bruckner W, Wetzig K and Genzel C 2001 *Surf. Coat. Technol.* **142** 861

[7] Wallin E, Selinder T I, Elfwing M and Helmersson U 2008 *EPL* **82**

[8] Yamada-Takamura Y, Koch F, Maier H and Bolt H 2001 *Surf. Coat. Technol.* **142** 260

[9] Jin P, Xu G, Tazawa M, Yoshimura K, Music D, Alami J and Helmersson U 2002 *J. Vac. Sci. Technol. A* **20** 2134
[10] Kyrylov O, Kurapov D and Schneider J M 2005 *Appl. Phys. A* **80** 1657
[11] Snyders R, Jiang K, Music D, Konstantinidis S, Markus T, Reinholdt A, Mayer J and Schneider J M 2009 *Surf. Coat. Technol.* **204** 215
[12] Kurapov D, Reiss J, Trinh D H, Hultman L and Schneider J M 2007 *J. Vac. Sci. Technol. A* **25** 831
[13] Wallin E, Munger E P, Chirita V and Helmersson U 2009 *J. Phys. D: Appl. Phys.* **42**
[14] Täschner C, Ljungberg B, Alfredsson V, Endler I and Leonhardt A 1998 *Surf. Coat. Technol.* **109** 257
[15] Ganciu M, Hecq M, Konstantinidis S, Dauchot J P, Touzeau M, de Poucques L and Bretagne J 2004 In: *World Patent No. WO 2005/090632,*
[16] Ganciu M, Konstantinidis S, Paint Y, Dauchot J P, Hecq M, de Poucques L, Vasina P, Mesko M, Imbert J C, Bretagne J and Touzeau M 2005 *J. Optoelectron. Adv. Mater.* **7** 2481
[17] Oliver W C and Pharr G M 1992 *J. Mater. Res.* **7** 1564
[18] Konstantinidis S, Jiang K and Schneider J M 2010 *unpublished*
[19] Zheng J, Sun B, Yang R, Song X B, Li X G and Pu Y K 2008 *J. Phys. Chem. B* **112** 12748
[20] Ramos R, Cunge G, Touzeau M and Sadeghi N 2008 *J. Phys. D: Appl. Phys.* **41** 115205
[21] Davis W D and Vanderslice T A 1963 *Phys. Rev.* **131** 219
[22] Ecker G and Müller K G 1961 *Z. Naturforsch., A: Phys. Sci.* **16** 246
[23] Dillon J A, Sheridan W F, Edwards H D and Ghosh S N 1955 *J. Chem. Phys.* **23** 776
[24] Langmuir I 1922 *Phys. Rev.* **21** 419
[25] Kohara T, Tamagaki H, Ikari Y and Fujii H 2004 *Surf. Coat. Technol.* **185** 166
[26] Hochauer D, Mitterer C, Penoy M, Michotte C, Martinz H P and Kathrein M 2008 *Surf. Coat. Technol.* **203** 350
[27] Gong J H, Peng Z J and Miao H Z 2005 *J. Eur. Ceram. Soc.* **25** 649
[28] Andersson J M, Czigany Z, Jin P and Helmersson U 2004 *J. Vac. Sci. Technol. A* **22** 117

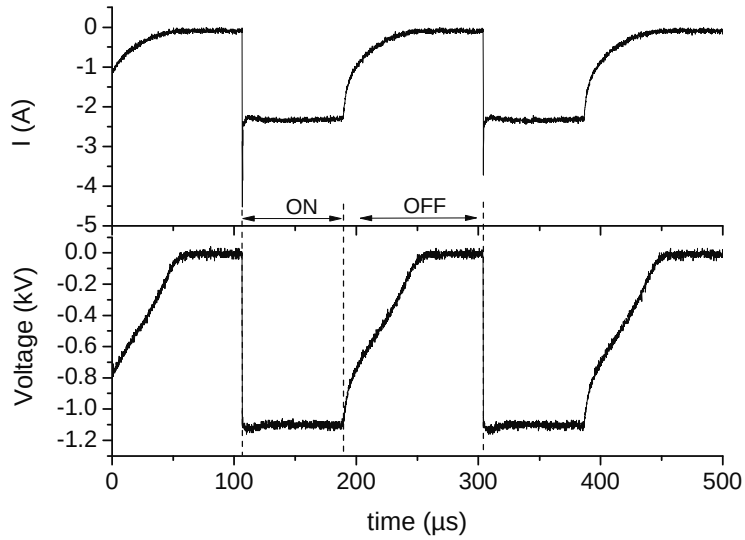

Figure 1. Time dependent cathode voltage (bottom panel) and current (top panel) of a discharge operating at a pulse width of 80 μs and a frequency of 5 kHz.

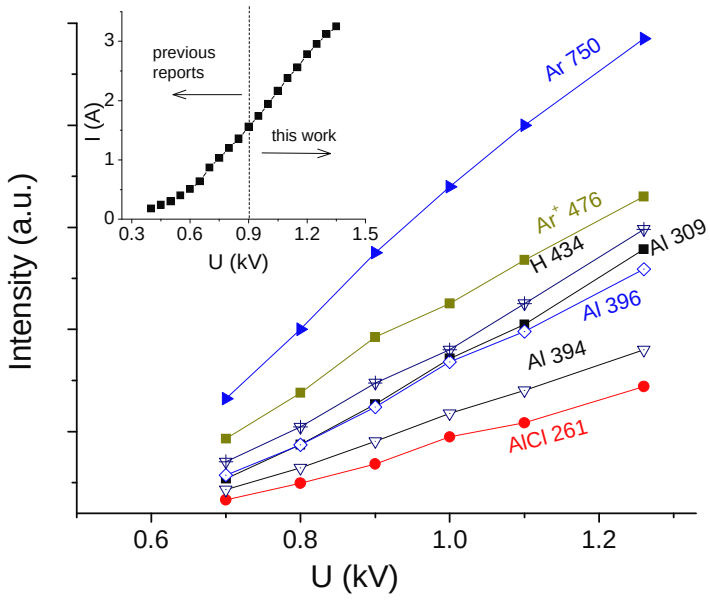

Figure 2. The intensity of the various emission lines versus the discharge voltage. The insert shows current-voltage curves recorded from the discharge operating the pulse width of 80 μs and frequency of 5 kHz.

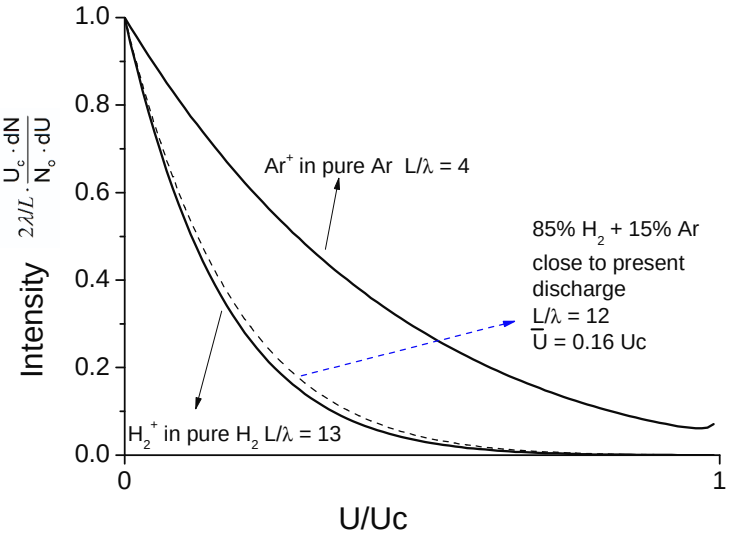

Figure 3. Ion energy distribution functions for pure Ar and H_2 plasmas (solid lines) and a plasma consisting of 85% H_2 and 15% Ar (dashed line).

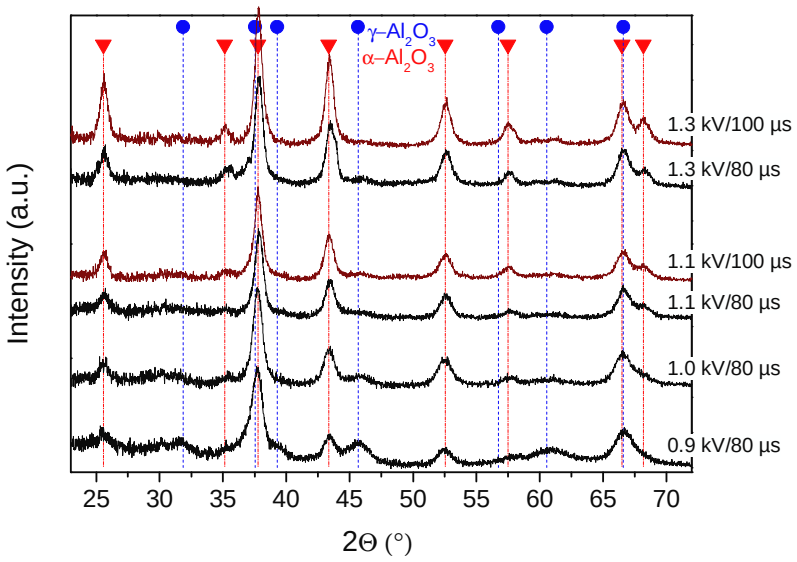

Figure 4. X-ray diffraction patterns of Al_2O_3 films deposited at various discharge voltages and pulse widths. The inverse triangles and the circles indicate the positions of the diffraction peaks associated with the presence of α- and γ-Al_2O_3, respectively.

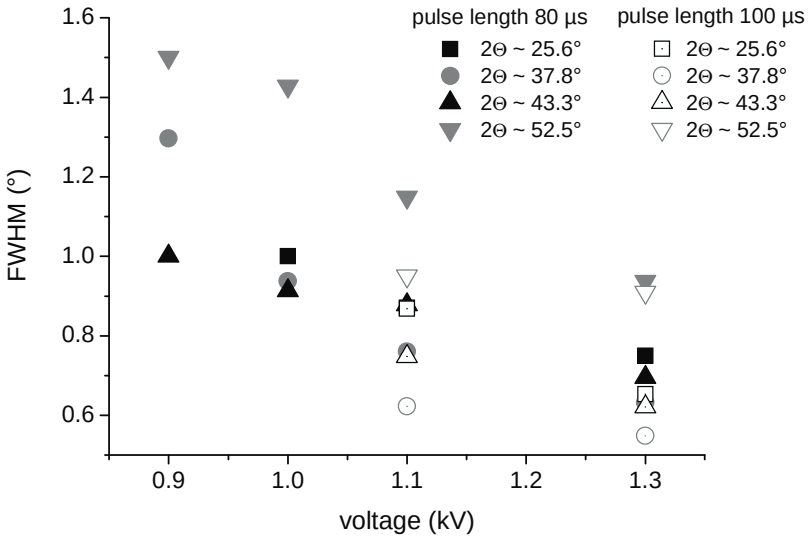

Figure 5. FWHM of chosen diffraction peaks as a function of various discharge voltages and pulse widths. Due to difficulty of peak fitting, data from sample deposited at 0.9 kV/80µs at 2θ ~25.6° is not shown.

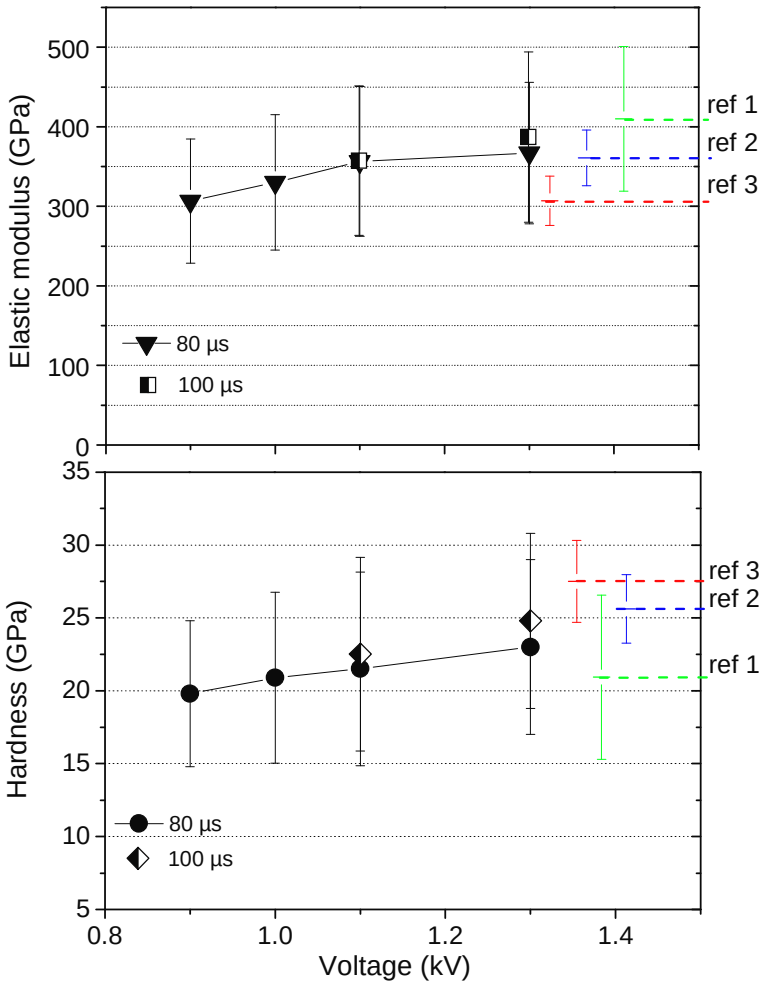

[1] Bulk nanocrystalline α-Al_2O_3[27]
[2] CVD α-Al_2O_3 film[26]
[3] RF sputtering α-Al_2O_3 film[28]

Figure 6. Elastic modulus (upper) and hardness (lower) of Al_2O_3 films as a function of the discharge voltage. The insert is a top view and the cross section SEM micrograph from a film deposited at a discharge voltage of 1.3 kV and a pulse width of 100 µs.

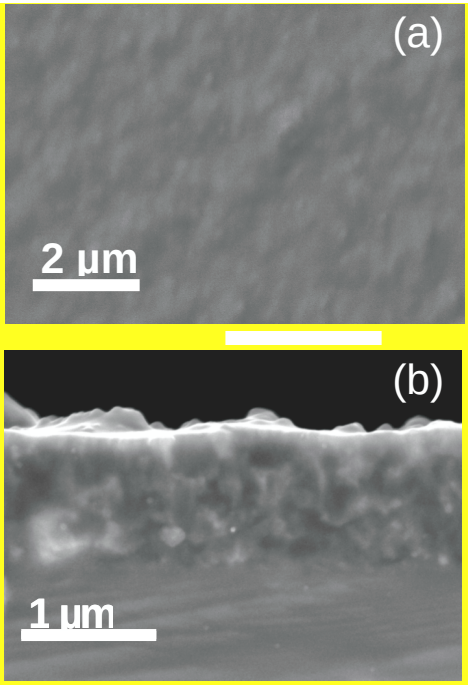

Figure 7. A top view (a) and a cross section (b) SEM micrograph from a film deposited at a discharge voltage of 1.3 kV and a pulse width of 100 µs.